ACS NANO

www.acsnano.org

Article

Nanopore Identification of Biogenic Amines and Its Applications in Food Freshness Evaluation

Yunqi Xiao,[§] Xiaoyu Du,[§] Lulu Zhao, Xinyi Dai, Lu Qian, Shanyu Zhang, Panke Zhang, Shuo Huang,* and Kefan Wang*

Cite This: *ACS Nano* 2026, 20, 2740−2751

Read Online

ACCESS | Metrics & More | Article Recommendations | Supporting Information

ABSTRACT: Biogenic amines (BAs) are nitrogenous biomolecules with essential physiological functions. However, excessive levels of BAs in food matrices can lead to adverse health effects. Conventional analytical techniques such as chromatography and mass spectrometry, are often limited by solvent dependency and derivatization requirements. Nanopore, an emerging single-molecule detection platform, was used to overcome these limitations. In this work, a single nickel ion-modified nanopore enabled the detection of aliphatic, aromatic, and heterocyclic BAs. Six BAs, including putrescine, cadaverine, β-phenylethylamine, tyramine, tryptamine and histamine were distinctly identified, with mechanistic insights elucidated via detailed event characterization. Furthermore, a machine learning classifier was developed for automated biogenic amine identification, achieving an accuracy of 99.0%. The strategy was also applied to detect BAs in real food samples, where five types of biogenic amines were successfully identified in shrimp, highlighting its significant potential for applications in food freshness monitoring and safety assurance.

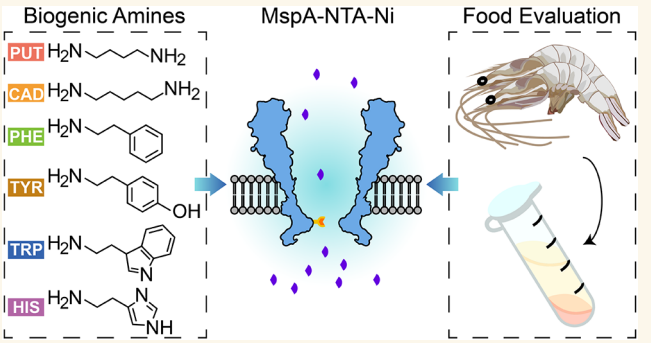

KEYWORDS: *biogenic amines, nanopore sensing, single-molecule, coordination chemistry, seafood spoilage*

INTRODUCTION

Biogenic amines (BAs) are organic nitrogenous compounds that play vital roles in various biological processes. Based on their chemical structures, BAs are classified as aliphatic, aromatic, and heterocyclic.[1] These compounds serve important physiological functions, such as acting as neurotransmitters in the regulation of key biological pathways.[2] BAs are also widely found in a variety of food products, such as meat,[3] seafood,[4] and fermented items.[5] Their formation in foods is primarily attributed to microbial decarboxylation of amino acids, a process favored in environments abundant in amino acids and supportive of microbial growth.[6] However, excessive intake of biogenic amines (BAs) may elicit toxicological effects. Accordingly, the detection of BAs is pivotal to identifying high-risk food products, thereby facilitating the implementation of regulatory oversight and production-related controls to mitigate excessive exposure and safeguard consumer health. Various conventional approaches have been employed for BA detection, including chromatographic techniques such as thin-layer chromatography (TLC)[7] and high-performance liquid chromatography (HPLC),[8−10] mass spectrometry such as matrix-assisted laser desorption/ionization mass spectrometry (MALDI-MS)[11,12] and ion mobility spectrometry,[13] as well as spectroscopy methods including spectrophotometry[14−16] and spectrofluorimetry.[17−20] In addition, techniques including enzymatic biosensors[21−23] and capillary electrophoresis (CE)[24−27] are also widely adopted for BA detection. Despite their widespread use, these methods exhibit limitations in terms of specificity, sensitivity, solvent requirement, instrumental complexity, and the need of time-consuming sample pretreatment and derivatization procedures.[28]

Nanopore is a novel single-molecule sensor that has been successfully used for the detection of a wide range of biomolecules,[29] such as nucleotides,[30,31] amino acids,[32−34] nucleic acids,[35,36] peptides,[37] proteins[38] and saccharides.[39,40] The recognition of BAs has been explored in solid-state nanopores.[41−43] Histamine was recognized by nitrilotriacetic acid-modified solid nanopores via an ion displacement mechanism.[41] Serotonin[42] and dopamine[43] were identified by aptamer-functionalized nanopores. Biological nanopore such as α-hemolysin (α-HL) was applied to investigate interactions between DNA hairpin structures and polyamines such as spermine, spermidine, and putrescine.[44] However, existing

Received: September 17, 2025
Revised: December 23, 2025
Accepted: January 6, 2026
Published: January 14, 2026

https://doi.org/10.1021/acsnano.5c16056
ACS Nano 2026, 20, 2740−2751

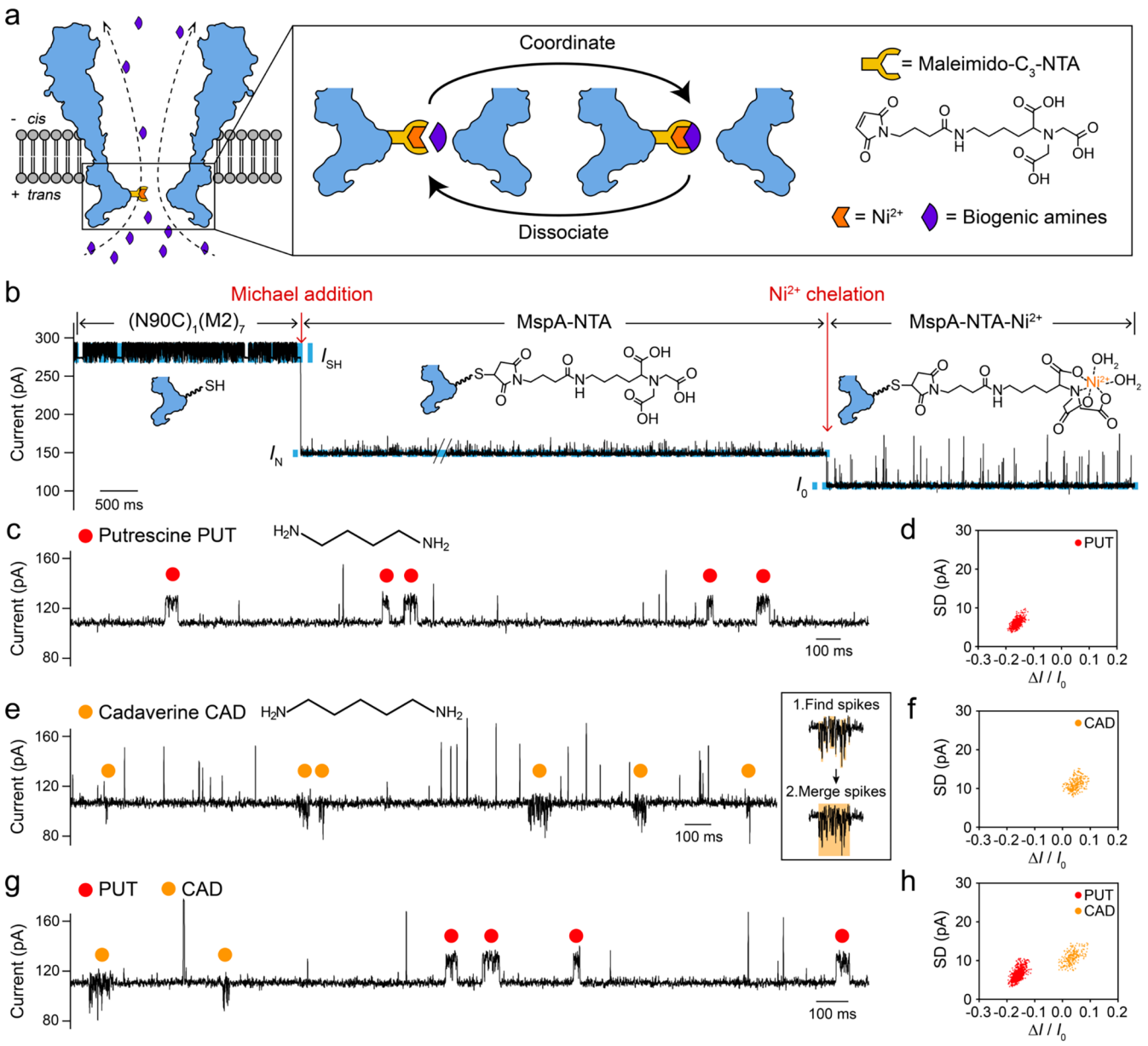

Figure 1. Biogenic amine (BA) sensing by MspA-NTA-Ni. (a) The schematic diagram of BA sensing using MspA-NTA-Ni. The Ni^{2+} was introduced by coordination with an NTA ligand, which was previously attached to the pore constriction. BAs could reversibly bind with the fixed Ni^{2+} to generate nanopore events. (b) Real-time monitoring of Ni-NTA modification. A maleimido-C3-NTA first reacts with $(N90C)_1(M2)_7$ via a Michael addition reaction to form MspA-NTA. Then, a Ni^{2+} was chelated by the NTA ligand to form MspA-NTA-Ni. Each current state transition, as marked by the red arrows, corresponding to a change into a different reaction state. I_0 represents the open pore current of MspA-NTA-Ni. (c) A representative trace of PUT sensing by MspA-NTA-Ni. PUT was added to *trans* with a final concentration of 10 mM. Sensing events of PUT were marked with red dots. (d) The scatter plot of $\Delta I/I_0$ vs *SD* of PUT sensing events ($n = 768$). (e) A representative trace of CAD sensing by MspA-NTA-Ni. CAD was added to *trans* with a final concentration of 10 mM. A split-merge strategy (Supporting Figure 7) was used to accurately find CAD sensing events (marked with orange dots). (f) The scatter plot of $\Delta I/I_0$ vs *SD* for CAD sensing events ($n = 258$). (g) A representative trace acquired during simultaneous sensing of PUT and CAD by MspA-NTA-Ni. PUT was added to *trans* with a final concentration of 4 mM. CAD was added to *trans* with a final concentration of 10 mM. Sensing events were identified and marked with red (PUT) or orange (CAD) dots. (h) The scatter plot of $\Delta I/I_0$ vs *SD* generated by results acquired by simultaneous sensing of PUT and CAD ($n = 1491$). The measurements in (b, c, e, g) were performed as described in Methods section in a 1.5 M KCl buffer (1.5 M KCl, 200 mM CHES, pH 9.0). A transmembrane potential of +100 mV was continuously applied.

nanopore systems have not achieved simultaneous discrimination of multiple BAs within a single platform. The development of a nanopore sensor capable of effectively distinguishing among different types of biogenic amines remains unrealized. This capability is crucial, as different BAs originate from distinct biological processes, and their identification is key to determining the type and severity of contamination. A multi-BA discriminable nanopore can deeply clarify the content of these toxic substances without separation and signal interference.

Engineered biological nanopores with tailored chemical reaction sites can expand their analytical capabilities. For example, the incorporation of Cu^{2+} into ligand-modified α-HL nanopore enabled the detection of six neurotransmitters[45] and five pairs of amino acid enantiomers.[32] *Mycobacterium smegmatis* porin A (MspA), an octameric protein nanopore with a conical

https://doi.org/10.1021/acsnano.5c16056
ACS Nano 2026, 20, 2740−2751

geometry,[46−48] has demonstrated significantly enhanced sensing performance for chemically active molecules and ions through the introduction of specific reaction sites within its constriction region.[49,50] Moreover, a heterogeneous MspA equipped with a single phenylboronic acid has been reported to identify nucleoside monophosphates,[30] monosaccharides[51] and alditol epimers.[52] In this work, a hetero-octameric MspA featuring an immobilized nickel ion at its pore constriction,[53] which has previously demonstrated ability to detect small molecules with metal-coordinating sites,[54,55] was used for sensing of BAs. Various BAs, including aliphatic, aromatic, and heterocyclic BAs were successfully detected, and the underlying sensing mechanisms were proposed. Distinctive events corresponding to different BAs were fully distinguished assisted with machine learning. This strategy was further applied to BA detection in shrimp samples, indicating its potential use in food freshness assessment.

BIOGENIC AMINE (BA) SENSING WITH A Ni^{2+}-MODIFIED MSPA NANOPORE

To site-specifically introduce a single Ni^{2+} into the nanopore for BA sensing (Figure 1a), a hetero-octameric MspA featuring a cysteine residue at its constriction, also referred to as $(N90C)_1(M2)_7$, was first prepared (Methods section).[30] A nitrilotriacetic acid (NTA) ligand was then covalently attached to the cysteine residue of $(N90C)_1(M2)_7$ via maleimide−thiol chemistry. A Ni^{2+} was subsequently chelated by the NTA, facilitating the formation of an NTA-Ni complex at the nanopore constriction. For simplicity, this NTA-Ni functionalized pore is referred to as MspA-NTA-Ni.[53] The stepwise modification process was monitored in real time using single-channel recording (Figure 1b). Experimentally, the measurement was performed with a custom measurement device with two chambers filled with a buffer of 1.5 M KCl and 200 mM (cyclohexylamino) ethanesulfonic acid (CHES) at pH 9.0 (Methods section). By convention, the electrically grounded chamber is defined as *cis* and the opposing chamber is defined as *trans*. A transmembrane potential of +100 mV was continually applied. Each chemical reaction step results in an irreversible current drop (Supporting Table 1). The open pore current of $(N90C)_1(M2)_7$ was 285.3 ± 7.2 pA (I_{SH}). The modification of maleimido-C_3−NTA cause the open pore current drop to 149.5 ± 1.9 pA (I_N). NTA chelation with Ni^{2+} caused a further current drop to 106.8 ± 1.9 pA (I_0), along with occasional background (BGD) events and transient spikes (Supporting Figure 1). To improve experimental efficiency, subsequent nanopore measurements were performed with batch-prepared MspA-NTA-Ni (Methods section), with the open pore current feature consistent with those observed during stepwise modification.

BAs are anticipated to reversibly bind with the immobilized NTA-Ni complex, yielding characteristic nanopore binding events (Figure 1a). To validate this, putrescine (PUT) and cadaverine (CAD) were selected as model BAs. They are aliphatic BAs derived from decarboxylation of ornithine and lysine, respectively. PUT and CAD could potentiate the toxicity of histamine (HIS) and serve as spoilage indicators.[56] Experimentally, upon the addition of PUT to the *trans* side of MspA-NTA-Ni at a final concentration of 10 mM, successive sensing events were immediately observed (Figure 1c). The rate of event appearance increased with higher PUT concentrations, confirming that the nanopore events were originated from PUT binding (Supporting Figure 2). PUT sensing could be also performed with addition in the *cis* chamber, however, the event frequency is markedly reduced compared to *trans*, as the electrophoretic force more effectively facilitates the positively charged molecules toward the pore from *trans* to *cis* the translocation of BAs into the pore from *trans* to *cis* (Supporting Figure 3). Therefore, all subsequent measurements were conducted with analytes added to *trans*, unless otherwise specified. No detectable nanopore events were observed when BA was sensed with M2MspA, confirming that the NTA-Ni located at the pore constriction is crucial for the generation of BA sensing events (Supporting Figure 4).

To quantitatively describe the sensing events, core parameters including the event dwell time (t_{off}), the interevent duration (t_{on}), the open pore current (I_0), the event current (I_{off}), the percentage blockage ($\Delta I/I_0 = (I_0 - I_{off})/I_0$), and the noise amplitude (SD) were defined in Supporting Figure 5. The mean values of $t_{off}(\tau_{off})$ and $t_{on}(\tau_{on})$ were derived from results of exponential fittings. Generally, the reciprocal of τ_{on} ($1/\tau_{on}$, $N = 3$) exhibits a linear correlation with analyte concentration, whereas the reciprocal of τ_{off} ($1/\tau_{off}$, $N = 3$) remains constant across different concentrations (Supporting Figure 2 and Table 2). $\Delta I/I_0$ and SD were used to visualize the sensing events (Figure 1d and Supporting Figure 6). A DBSCAN (density-based spatial clustering of applications with noise) algorithm was applied to filter out nonclustered noise events, followed by manual removal of BGD events intrinsic to MspA-NTA-Ni (Supporting Figure 1). Based on three independent replicates ($N = 3$), the above-described sensing events generate highly reproducible data (Supporting Figure 6 and Supporting Table 3), demonstrating the robustness of MspA-NTA-Ni in BA sensing.

Similarly, CAD was also detectable by MspA-NTA-Ni, with event shapes distinct from those of PUT (Figure 1e). Notably, the low amplitude of CAD events poses challenges for discrete event extraction from continuous current traces using the conventional "Single-channel Search" function in Clampfit. To address this, a split-merge strategy was adopted to accurately search CAD events (Methods section), in which each event was split into multiple spikes and subsequently reconstructed into a complete event based on temporal intervals (Figure 1e and Supporting Figure 7). After cluster analysis and BGD removal, the scatter plot of $\Delta I/I_0$ *versus* SD of CAD sensing events shows a single and narrowly distributed populations (Figure 1f and Supporting Figure 8).

The event characteristics kept steady and event rate up-regulated when CAD concentration increased (Supporting Figure 9). A deeper current blockade was observed for CAD compared to PUT, likely due to the additional methylene group in CAD enhancing the steric exclusion at the pore constriction. This interpretation is strongly supported by measurements of 1,6-hexanediamine (Supporting Figure 10), which extends the carbon backbone by one more methylene unit and produces a correspondingly deeper current blockage (Supporting Figure 11).

To examine the capability of MspA-NTA-Ni for simultaneous discrimination of PUT and CAD, sensing measurement was performed with both PUT and CAD present. Stochastic sensing events of PUT and CAD were observed during the measurement (Figure 1g). Following background reduction, the scatter plot revealed two clearly separated event distributions (Figure 1h and Supporting Figure 12), consistent with the results obtained from individual BA sensing. These results confirm the superior resolution of MspA-NTA-Ni in real-time discrimination of BAs.

https://doi.org/10.1021/acsnano.5c16056
ACS Nano 2026, 20, 2740−2751

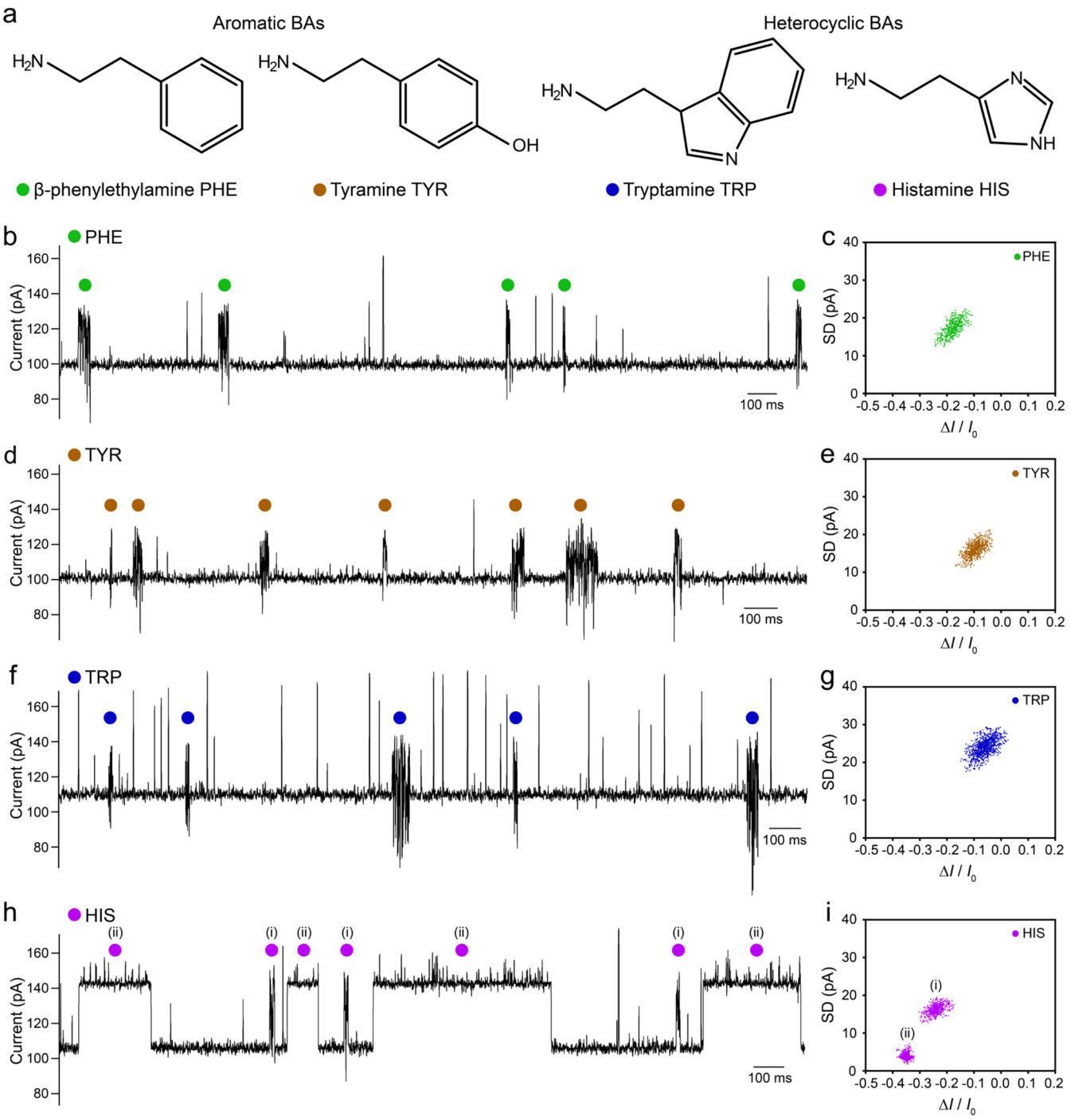

Figure 2. Single-molecule detection of PHE, TYR, TRP and HIS. (a) The chemical structures of PHE, TYR, TRP and HIS. PHE and TYR are aromatic BAs, while TRP and HIS are heterocyclic BAs. (b) A representative trace of PHE sensing by MspA-NTA-Ni. PHE was added to *trans* with a final concentration of 10 mM. Sensing events of PHE were marked with green dots. (c) The scatter plot of $\Delta I/I_0$ vs *SD* for PHE sensing events (n = 525). (d) A representative trace of TYR sensing by MspA-NTA-Ni. TYR was added to *trans* with a final concentration of 10 mM. Sensing events of TYR were marked with brown dots. (**e**) The scatter plot of $\Delta I/I_0$ vs *SD* for TYR sensing events (n = 684). (f) A representative trace of TRP sensing by MspA-NTA-Ni. TRP was added to *trans* with a final concentration of 10 mM. Sensing events of TRP were marked with blue dots. (g) The scatter plot of $\Delta I/I_0$ vs *SD* for TRP sensing events (n = 904). (h) A representative trace of HIS sensing by MspA-NTA-Ni. HIS was added to *trans* with a final concentration of 800 μM. Sensing events of HIS were marked with purple dots. Two types of events were observed during HIS sensing. The events with short t_{off} were marked with (i) and the events with long t_{off} were marked with (ii). (i) The scatter plot of $\Delta I/I_0$ vs *SD* for HIS sensing events (n = 1926). The two types of events can be clearly distinguished. All measurements in Figure 2 were performed as described in Methods section in a 1.5 M KCl buffer (1.5 M KCl, 200 mM CHES, pH 9.0). A transmembrane potential of +100 mV was continuously applied.

https://doi.org/10.1021/acsnano.5c16056
ACS Nano 2026, 20, 2740−2751

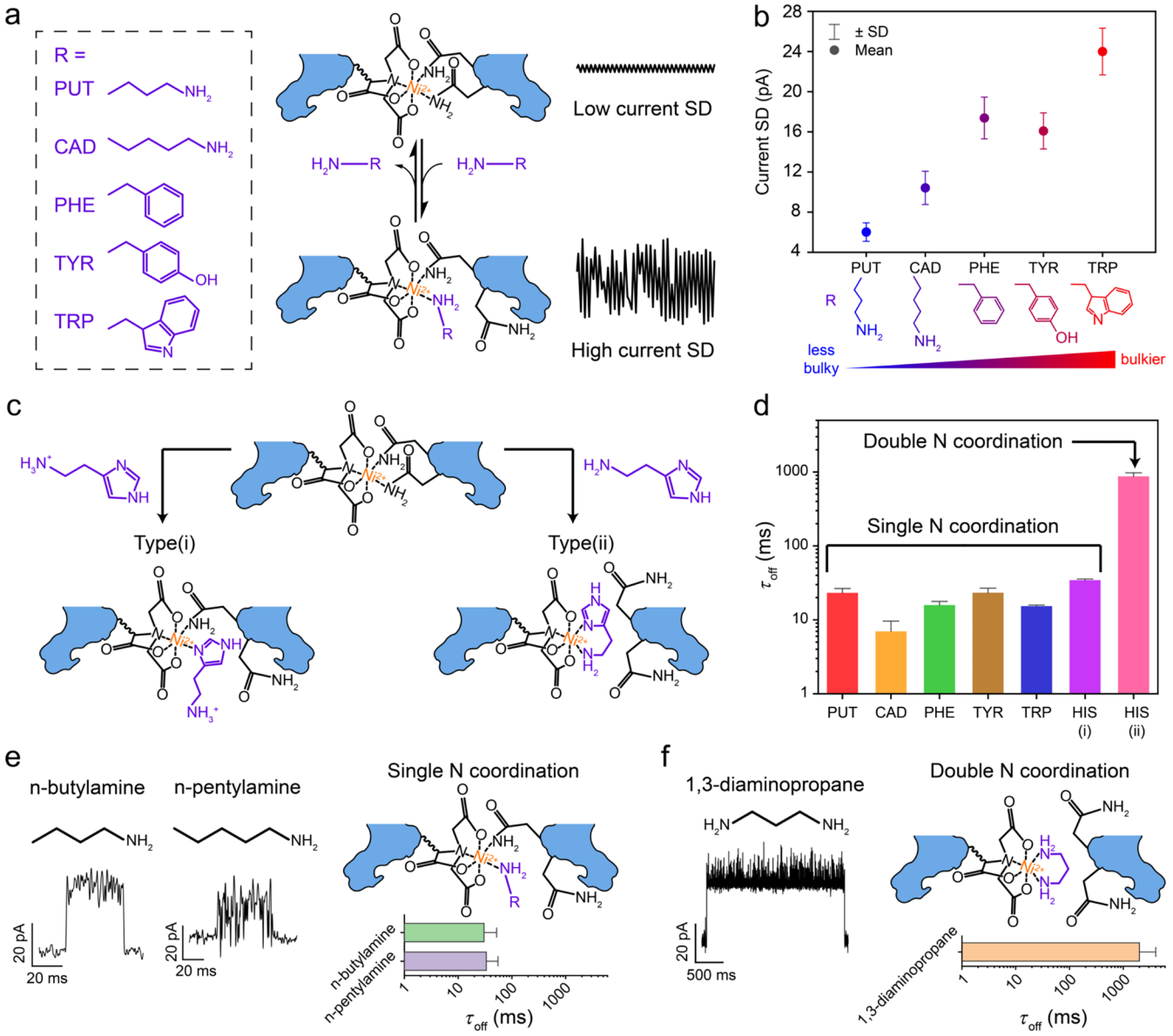

Figure 3. Single-molecule coordination mechanisms of amines with MspA-NTA-Ni. (a) A proposed coordination mechanism for PUT, CAD, PHE, TYR and TRP. Within MspA-NTA-Ni, Ni^{2+} is coordinated by four bonds from NTA, leaving two orbitals occupied by amide groups inside the protein pore. This configuration exhibits a low current standard deviation. The primary amine group of BAs can reversibly displace the amide group to coordinate with Ni^{2+}, resulting in a transition to a high current standard deviation state, recorded as a sensing event. (b) The interval plot of current *SD* for the five BAs shown in (a). Bulkier BAs tend to generate higher current *SD* during coordination. Error bars represent the standard deviation of the current *SD* (c) A proposed coordinating mechanism for HIS. The primary amine of HIS was partially protonated under the experimental condition (pH 9.0). Protonated HIS primarily coordinates via the imidazole ring (type (i)), whereas deprotonated HIS utilizes both the primary amine and the imidazole group to form a stable six-membered chelate ring with Ni^{2+} (type (ii)). (d) The bar plot of τ_{off} for different BA event types. The values and error bars represent the mean and standard deviation, generated from results of three independent measurements ($N = 3$). (e) Sensing of *n*-butylamine and *n*-pentylamine. Both analytes report single event type with τ_{off} in the millisecond to tens of milliseconds range, consistent with a monodentate mode. The error bars represent the standard deviation of τ_{off}. (f) Sensing of 1,3-diaminopropane. 1,3-Diaminopropane reports single event type with τ_{off} on the order of seconds, supporting a bidentate coordination mode. The error bars represent the standard deviation of τ_{off}.

IDENTIFICATION OF AROMATIC AND HETEROCYCLIC BAS

The sensing capacity of MspA-NTA-Ni was further expanded to the sensing of *β*-phenylethylamine (PHE), tyramine (TYR), tryptamine (TRP) and histamine (HIS). PHE and TYR are aromatic BAs, while TRP and HIS belong to heterocyclic BAs (Figure 2a). These BAs are respectively generated by decarboxylation of phenylalanine, tyrosine, tryptophan, and histidine. HIS is primarily associated with nervous system, whereas PHE, TYR and TRP play regulatory roles in vascular system.[6,57] HIS exerts its biological effects by binding to four subtypes of membrane receptors.[58] PHE acts as a stimulant that promotes the release of neurotransmitters.[59] TYR is a vasoactive amine that effects on blood vessel activity.[60] TRP exhibits significant neurological functions.[61] HIS and TYR are considered the most biologically active amines[57,62] and are recognized as major contributors to food poisoning incidents.[5]

All measurements were performed under the same conditions as those for PUT and CAD (Figure 1). PHE, TYR, TRP and HIS

https://doi.org/10.1021/acsnano.5c16056
ACS Nano 2026, 20, 2740−2751

were separately added to *trans* to initiate nanopore measurement. For effective data collection, the concentration of each analyte was adjusted to yield a sufficiently high event frequency. At a concentration of 10 mM, PHE, TYR, and TRP each produced a single type of sensing event (Figure 2b−g), whereas HIS produced a considerable event frequency and displayed two distinct event types at a lower concentration of 0.8 mM (Figure 2h,i). Based on three independent measurements ($N = 3$) with each BA, the above-described sensing events generate highly reproducible data (Supporting Figures 13−16). The generated core event parameters summarized in Supporting Table 3 list the quantitative details. The concentration dependence measurements show the increased event rate with BA concentration rising (Supporting Figures 17−20 and Table 2). The positive correlation between the event capture rate and the analyte concentration across all BAs examined indicates that events were generated from BA interaction with MspA-NTA-Ni (Supporting Figures 2, 9, 17−20). The linear correlation is also critical for quantitative BA analysis using nanopore. To definitively confirm that event generation originates from BA binding to the nickel ion, sensing experiments using an MspA-NTA pore without the Ni^{2+} ion were performed. The absence of any detectable events with MspA-NTA stands in sharp contrast to the robust events obtained with the MspA-NTA-Ni pore (Supporting Figure 21). This result unequivocally demonstrates that the coordinated nickel ion is indispensable for BA interaction and event generation.

Further exploration into the capture mechanisms of BAs has revealed distinct transport behaviors. The capture of small molecules, particularly neutral species, by nanopores constitutes a complex physical process involving multiple physical effects. While charged molecules are predominantly driven by electrophoretic forces, the transport of neutral species involves a combination of electroosmotic flow, diffusion, dielectrophoresis.[63−67] To systematically elucidate the driving forces underlying BA capture, voltage-dependent assays were conducted using PUT, which is positively charged and PHE, which is neutral, as representative analytes (Supporting Figures 22−24). Experimentally, the event frequency of PUT was significantly enhanced at positive voltages compared to negative potentials (Supporting Figure 22), indicating a significant contribution from the electrophoretic force. In contrast, the event appearance rate of PHE exhibited a slight voltage-dependence in event frequency (Supporting Figure 23), suggesting a minor electroosmotic force. Furthermore, both charged and neutral BAs continued to produce well-defined nanopore binding events even under near-zero applied voltage (Supporting Figure 24), suggesting that diffusion is a universal factor that drives BAs into the pore constriction for molecular adapter binding. Collectively, these results demonstrate that neutral BAs are primarily transported by diffusion and electroosmotic force, while positively charged species are driven by a combination of predominant electrophoretic force, diffusion and electroosmotic force.

COORDINATION MECHANISMS OF DIFFERENT BAS WITH MSPA-NTA-NI

Inspired by the different event types observed across different BAs, it is hypothesized that these variations originate from different coordination mechanisms between BAs and MspA-NTA-Ni. In the absence of analyte, Ni^{2+} induces strong interactions between the NTA adapter and the amide groups within the pore lumen, resulting in a tightly constrained configuration that exhibits a stable open pore current with low current noise (Figure 3a). Binding with BA such as PUT, CAD, PHE, TYR or TRP disrupts the interaction between NTA-Ni and pore lumen, as Ni^{2+} becomes coordinated with the primary amine group of the BA. This monodentate binding triggers a reconfiguration of the molecular adapter while maintaining the complex near the pore constriction (Figure 3a), a region where the ionic current is highly sensitive to the molecular variations. Consequently, BAs with bulkier side chains generally induce more significant current fluctuations, whereas PUT, as the smallest analyte in the series, yields minimal current noise (Figure 3b). However, the current noise is impacted by not only the steric volume of the analyte but also a variety of analyte-pore interactions such as hydrophilicity and dynamic flexibility. With a phenolic hydroxyl group, the event *SD* of TYR deviates slightly from the overall trend (Figure 3b). Presumably, the hydrophilic moiety potentially altered the molecule's solvation shell and its orientation or configuration when bound to the Ni^{2+} center, which reduced the effective dynamic volume and conformational fluctuations that contribute to current noise. These findings confirm the excellent resolution of MspA-NTA-Ni in distinguishing subtle structural differences among BAs.

Unlike the aforementioned BAs, HIS features two potential coordination sites, the primary amine group and the imidazole ring. This structure enables HIS to adopt multiple coordination modes with the fixed NTA-Ni adapter, thereby generating multiple types of sensing events (Figure 2h). Under the experimental conditions, the imidazole nitrogen was fully deprotonated, while the primary amine was partially protonated. In the protonated state, HIS likely engages in monodentate coordination via the imidazole moiety, corresponding to event type (i) observed during nanopore measurements (Figure 3c). In the deprotonated state, HIS acts as a bidentate ligand, coordinating simultaneously via both the imidazole and primary amine to form a stable six-membered chelate ring, which manifests as an extended dwell time characteristic of event type (ii) (Figure 3c). Presumably, this tight bidentate binding fully released the adapter from the pore constriction, thereby reducing the current sensitivity to molecular motions and yielding the relatively low levels of current noises. To verify the two coordination states of HIS, various pH conditions were used to regulate the protonation state of primary amine. As the pH drops from 9 to 6, the ratio and dwell time of event type (ii) decreased notably (Supporting Figure 25), which is consistent with the fact that the protonation ratio of primary amines increases. Notably, although PUT and CAD possess two primary amines, they do not act as bidentate ligand coordination like HIS due to the coordination geometry constraints.

The dissociation kinetics of different BA event types were further characterized. As shown in Figure 3d, the event τ_{off} for PUT, CAD, PHE, TYR, TRP and HIS (i) ranged from milliseconds to tens of milliseconds, while HIS (ii) exhibited τ_{off} extending into seconds, suggesting that single-nitrogen coordination is markedly weaker than double-nitrogen coordination. Validation experiments using *n*-butylamine, *n*-pentylamine, and 1,3-diaminopropane under identical conditions further corroborated these observations. Both *n*-butylamine and *n*-pentylamine, as monoamines, demonstrate event τ_{off} similar to those of BA employing single-N coordination (Figure 3e and Supporting Figures 26, 27). In contrast, sensing events acquired with 1,3-diaminopropane demonstrate τ_{off} on the order of seconds, consistent with a bidentate coordination mode (Figure 3f and Supporting Figure 28). These results demonstrate the

https://doi.org/10.1021/acsnano.5c16056
ACS Nano 2026, 20, 2740−2751

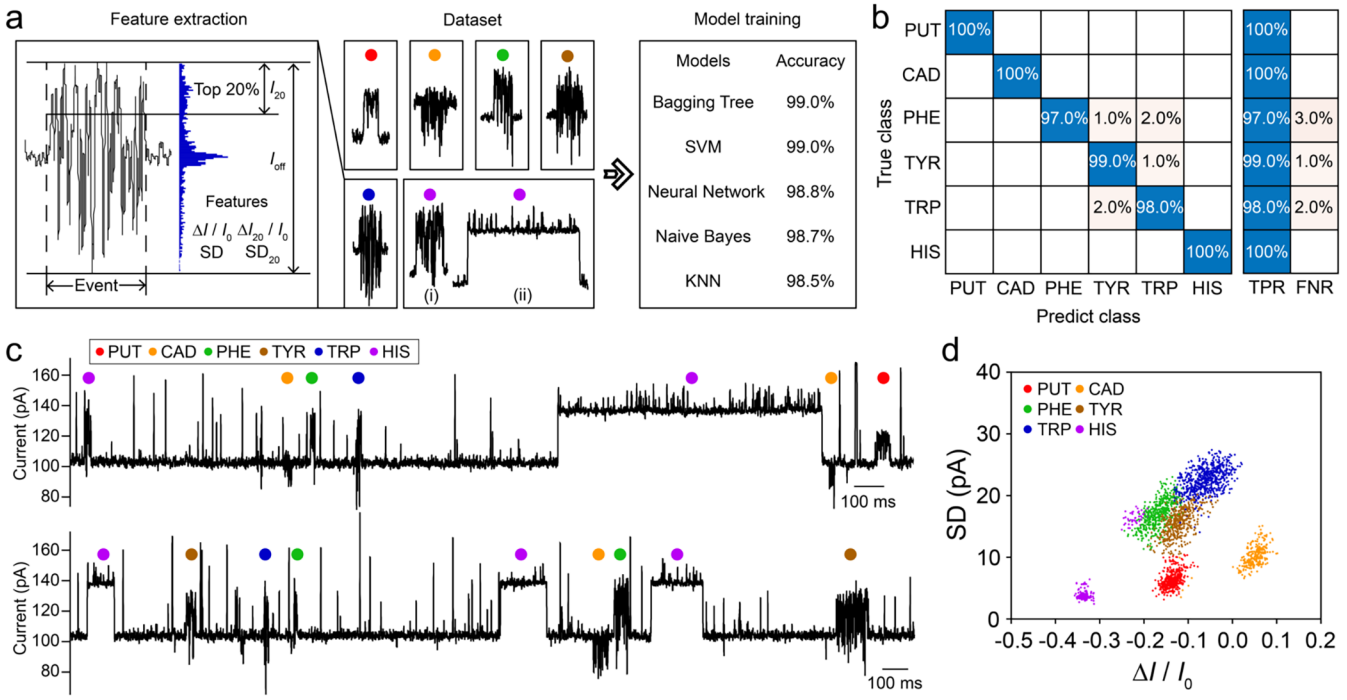

Figure 4. Machine learning assisted identification of six BAs. (a) The workflow of machine learning. Sensing events separately from six BAs were collected to construct a labeled data set. Four event features ($\Delta I/I_0$, *SD*, $\Delta I_{20}/I_0$, and SD_{20}) were extracted from each event for machine learning. Model training was performed by all default classifiers in the Classification Learner toolbox of MATLAB, with Bagging Tree and SVM achieving the highest testing accuracy (99.0%). The Bagging Tree model was selected for subsequent prediction. (b) The confusion matrix of BA classification generated by Bagging Tree model using the testing set. (c) Representative traces acquired during simultaneous sensing of six BAs by MspA-NTA-Ni. The measurements were performed as described in Methods section in a 1.5 M KCl buffer (1.5 M KCl, 200 mM CHES, pH 9.0). A transmembrane potential of +100 mV was continuously applied. Six BAs were simultaneously added to *trans* (final concentrations: PUT, 4 mM; CAD, 10 mM; PHE, 2 mM; TYR, 5 mM; TRP, 3 mM; HIS, 100 μM). The events were automatically predicted by the trained Bagging Tree model. (d) The scatter plot of $\Delta I/I_0$ vs *SD* generated by results acquired during simultaneous sensing of six BAs (n = 2547). All event identities were predicted by the trained Bagging Tree model and labeled with color-coded dots.

utility of MspA-NTA-Ni for evaluating coordination stability and elucidating binding modes of amine ligands.

MACHINE LEARNING-ASSISTED BA CLASSIFICATION

The characteristic event signatures of different BAs facilitated their automated classification using supervised machine learning approaches. A labeled data set was constructed with 500 events per BA class. Four event features ($\Delta I/I_0$, *SD*, $\Delta I_{20}/I_0$, and SD_{20}) were extracted for each event to form a feature matrix (Figure 4a). Here, two new features ($\Delta I_{20}/I_0$ and SD_{20}) were introduced to enhance event description (Supporting Figure 29). ΔI_{20} and SD_{20} are defined as the mean value and the standard deviation of the top 20% of the event current, respectively. The feature matrix was then randomly split into a training set (80%, 400 events per BA) for model training and a testing set (20%, 100 events per BA) for model testing. Machine learning was performed using the Classification Learner toolbox of MATLAB (Methods section), seven inbuilt classifiers were evaluated. The Bagging Tree model and Support Vector Machine (SVM) model achieved the highest accuracy of 99.0% (Figure 4a). Both models report satisfying accuracy for event prediction. The Bagging Tree model had a slightly higher precision than the SVM model (Supporting Figure 30). Therefore, the Bagging Tree model was selected for further prediction and its confusion matrix was shown in Figure 4b, in which all BA events demonstrate a minimum true-positive rate (TPR) of 97%. An impressive TPR of 100% was achieved by PUT, CAD and HIS. Compared with the Bagging Tree model trained by two features ($\Delta I/I_0$, *SD*), the two additional features ($\Delta I_{20}/I_0$, SD_{20}) effectively improved the accuracy of the model (Supporting Figure 31).

Furthermore, the trained Bagging Tree model was used to identify unlabeled BA events obtained from a mixture of six BAs. All sensing events acquired from results of simultaneous sensing experiments were processed by the split-merge strategy (Supporting Figure 32). Following feature extraction and background reduction (Supporting Figure 33), sensing events were recognized by the trained Bagging Tree model (Figure 4c and Supporting Movie 1). The corresponding scatter plot of $\Delta I/I_0$ *versus* *SD* after machine learning prediction was shown in Figure 4d. Event distributions of different BAs were clearly revealed.

DETECTION OF BAS IN SHRIMP

BAs are widely present in dietary food such as fish, meat, wine and beer.[1] They have toxicological effects on humans, with HIS being particularly notable, while PUT, CAD and TYR are known to potentiate HIS toxicity. Seafood, including fish and shellfish, is a primary source of multiple BAs, and their levels serve as critical indicators for evaluating food safety and quality.[56] Therefore, detection of BAs in seafood is essential for monitoring food freshness and mitigating potential health risks associated with their consumption.

To demonstrate the feasibility of BA detection in a real-world sample using nanopores, rotten shrimps were analyzed with

https://doi.org/10.1021/acsnano.5c16056
ACS Nano 2026, 20, 2740−2751

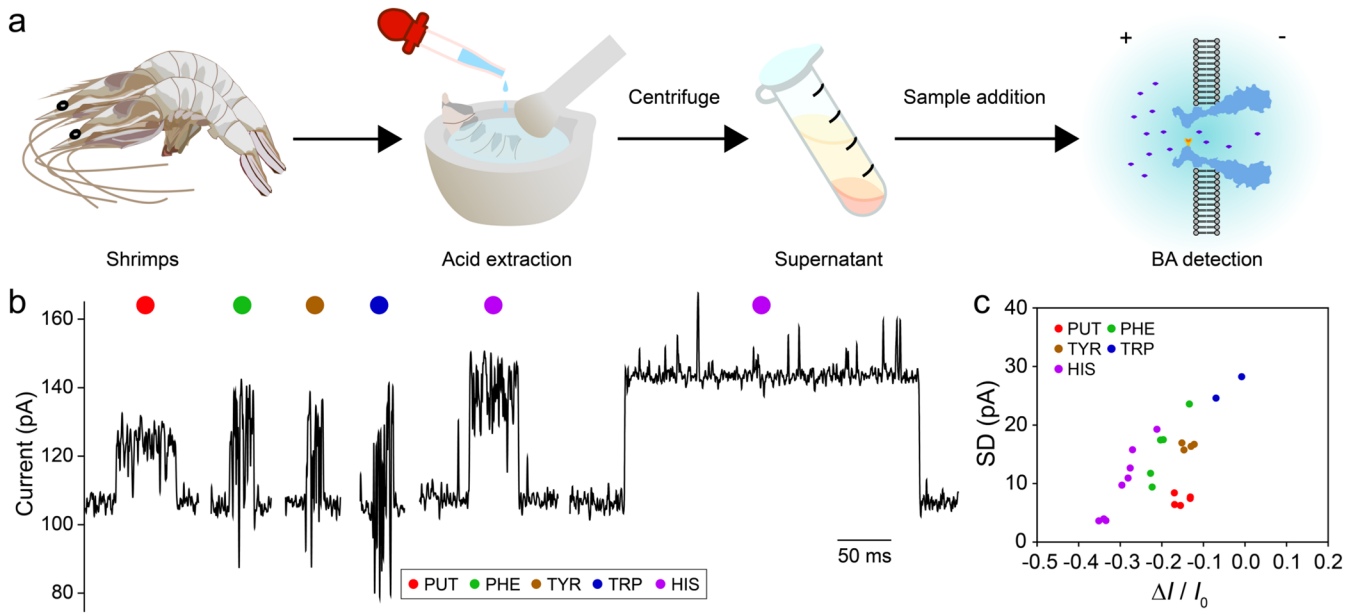

Figure 5. Identification of BAs in shrimps. (a) A flow diagram of BA detection in shrimp by MspA-NTA-Ni. The shrimp was soaked with TCA and ground for BA extraction. The mixture was centrifuged after pH adjustment to 8−9. The supernatant was then subjected to MspA-NTA-Ni for BA detection. (b) Representative events of BAs detected in shrimp. The measurements were performed as described in Methods section in a 1.5 M KCl buffer (1.5 M KCl, 200 mM CHES, pH 9.0). A transmembrane potential of +100 mV was continuously applied. Ten μL of supernatant was added to *trans*. Events of PUT (red), PHE (green), TYR (brown), TRP (blue) and HIS (purple) were identified. (c) The scatter plot of $\Delta I/I_0$ vs *SD* of detected BA events (n = 24). The event identities were predicted by the trained Bagging Tree model.

MspA-NTA-Ni (Figure 5a). Experimentally, the rotten shrimp was crushed in 0.4 M trichloroacetic acid (TCA) to extract BAs, after which the mixture was adjusted to pH 8−9 and centrifuged to obtain the supernatant (Methods section). With a single MspA-NTA-Ni, 10 μL of supernatant was added to *trans* to initiate nanopore measurement. Different types of BA events were immediately observed during single-channel recording. The identities of all acquired BA events were automatically recognized by the pretrained Bagging Tree model, where PUT, PHE, TYR, TRP and HIS were successfully identified (Figure 5b,c). The event characteristics of BAs detected in shrimp were fully consistent with those obtained from pure compounds. All relevant BA events from the raw traces are shown in Supporting Figure 34. This agreement underscores the single-molecule sensitivity of the sensing mechanism and highlights the high specificity afforded by the NTA-Ni adapter. The limit of detection and limit of quantitation for all six BAs are also determined (Supporting Table 4). Furthermore, this method was applied to the concentrated shrimp sample extract by MspA-NTA-Ni. Robust detection was achieved for cadaverine (CAD) and five additional target BAs (PUT, PHE, TYR, TRP, HIS). Notably, by sample enrichment, the event frequency of all BAs was significantly elevated in this real-world sample (Supporting Figure 35a). After accounting for interference from unknown events, the concentrations of the target BAs were quantified using the established calibration curves (Supporting Figures 2, 9, 17−20), and the quantitative results were consistent with those obtained via LC-MS (Supporting Figure 35b). These findings demonstrate that MspA-NTA-Ni can provide a comprehensive spoilage profile of the tested food sample.

CONCLUSIONS

In summary, a single Ni^{2+} modified nanopore (MspA-NTA-Ni) was reported to detect biogenic amines (BAs). Six representative BAs, spanning aliphatic, aromatic, and heterocyclic classes, were successfully detected and distinguished. Based on the chemical structures and diverse event profiles of the BAs, different coordination modes between MspA-NTA-Ni and the analytes were proposed. The event noise was found to correlate with the molecular size of BAs, highlighting the high resolution of MspA-NTA-Ni in discriminating subtle structural differences. In contrast, a longer dwell time was observed for BAs engaging in bidentate coordination, indicating higher complex stability compared to monodentate binding. The transformation between monodentate and bidentate coordination can be monitored by the pH-dependent protonation state. The monodentate and bidentate binding signature in MspA-NTA-Ni provided deep insight in single-molecule coordination. A machine learning-based classifier was established to automate BA event identification, with which a general classification accuracy of 99.0% was reported. This sensing strategy was further applied in BA detection in real shrimp samples, from which BAs were successfully identified and quantified. The comparable quantification result with LC-MS suggesting its credible application in freshness monitoring in food industry. Beyond biogenic amines, this approach could be extended to detect other nonbiogenic amines, facilitating the exploration of diverse coordination mechanisms with single-molecule precision.

METHODS

Preparation of $(N90C)_1(M2)_7$

The hetero-octameric MspA, referred to as $(N90C)_1(M2)_7$, consists of one monomer of N90C MspA-H6 and seven monomers of M2MspA-D16H6.[30] To prepare this assembly, the genes encoding N90C MspA-H6 and M2MspA-D16H6 were coexpressed in the pETDuet-1 vector. Both genes were engineered with a C-terminal hexahistidine tag (H6) for purification via nickel affinity chromatography, while M2MspA-D16H6 additionally featured a 16-aspartate tag (D16) to facilitate electrophoretic discrimination of $(N90C)_1(M2)_7$.

https://doi.org/10.1021/acsnano.5c16056
ACS Nano 2026, 20, 2740−2751

For expression, 100 ng of plasmid was transformed into 100 μL *Escherichia coli* BL21 (DE3) pLysS competent cells and heat-shocked at 42 °C for 90 s. After recovery in LB medium, cells were plated on agar containing ampicillin (50 μg/mL) and chloramphenicol (34 μg/mL) and cultured at 37 °C for 18 h. A single colony was inoculated into LB broth under the same antibiotic conditions, cultured to OD_{600} ∼ 0.6−0.8, and scaled up to 1 L. Protein expression was induced with 0.1 mM IPTG at 16 °C for 24 h. Cells were harvested by centrifugation at 4500 rpm for 20 min at 4 °C.

The collected pellet was resuspended in lysis buffer (100 mM Na_2HPO_4/NaH_2PO_4, 0.1 mM EDTA, 150 mM NaCl, 0.5% (v/v) Genapol X-80, pH 6.5), heated at 65 °C for 50 min, and centrifuged at 13,000 rpm for 1 h at 4 °C. The supernatant was filtered (0.2 μm) and loaded onto a HisTrap HP column. After washing with buffer A (0.5 M NaCl, 20 mM HEPES, 5 mM imidazole, 2 mM TCEP, 0.5% (v/v) Genapol X-80, pH 8.0), bound proteins were eluted using a linear gradient of buffer B (0.5 M NaCl, 20 mM HEPES, 500 mM imidazole, 2 mM TCEP, 0.5% (v/v) Genapol X-80, pH 8.0). Fractions containing MspA assemblies were identified by a 4−20% gradient SDS−polyacrylamide gel. $(N90C)_1(M2)_7$ was further purified by 10% SDS−polyacrylamide gel (+160 V, 16 h). After Coomassie staining and destaining, the protein band of $(N90C)_1(M2)_7$ was excised from the gel and immersed with extraction solution (150 mM NaCl, 15 mM Tris-HCl, pH 7.5, 0.2% DDM, 0.5% Genapol X-80, 5 mM TCEP, 10 mM EDTA) for 12 h. The extracted $(N90C)_1(M2)_7$ was stored at − 80 °C for long-term use.

Preparation of MspA-NTA-Ni

To modify $(N90C)_1(M2)_7$ with a nitrilotriacetic acid (NTA), 8 μL of 20 mM maleimido-C3-NTA was mixed with 1 μL of purified $(N90C)_1(M2)_7$ and incubated for 1 week at −80 °C. The resulting product is referred to as MspA-NTA. Before nanopore measurements, the MspA-NTA solution was mixed with 0.1 μL of 100 mM $NiSO_4$ and incubated at room temperature for 5 min to generate MspA-NTA-Ni.

Nanopore Measurements

Nanopore measurements were performed as described previously.[50] To minimize environmental interference, the custom measurement device was housed in a Faraday cage mounted on an optical table (Jiangxi Liansheng Technology Co., Ltd.). The two chambers of the measurement device were separated by a Teflon film containing a central orifice (∼100 μm diameter). Prior to measurements, the orifice was treated with 2% (v/v) hexadecane in pentane. Both chambers were then filled with 500 μL of 1.5 M KCl buffer (1.5 M KCl, 200 mM CHES, pH 9.0). A pair of Ag/AgCl electrodes connected to a patch-clamp amplifier were immersed in the KCl buffer in each chamber. Conventionally, the grounded chamber is defined as *cis* while the opposing chamber is defined as *trans*. A drop of DPhPC (diphytanoylphosphatidylcholine, 5 mg/mL in pentane) was then added to each chamber to form a lipid bilayer on the orifice. Then, nanopores were added to *cis* to trigger spontaneous pore insertions. Upon a single nanopore insertion, the buffer in *cis* was replaced with fresh KCl buffer to avoid additional pore insertions. Unless specified, all analytes were added to the *trans* chamber to a desired concentration.

All single-channel recordings were performed with an Axonpatch 200B patch-clamp amplifier coupled with a Digidata 1550B digitizer. Data were acquired at 25 kHz sampling rate with 1 kHz low-pass filtering. Unless specified, a transmembrane potential of +100 mV was continuously applied during all measurements. Representative traces were further low-pass filtered with a frequency of 500 Hz (Bessel, 8-pole) using Clampfit 10.7 for demonstration purposes.

Data Processing and Analysis

Event extraction and analysis were performed using Clampfit 10.7 and MATLAB R2021a. The extraction workflow consists of spike detection, spike merging, and event screening (Supporting Figure 7). Spike detection was conducted using the 'Single-Channel Search' function in Clampfit 10.7, with an ignore duration set to 0.4 ms. Spike emerging was accomplished through a MATLAB program, where spikes separated by intervals less than 4 ms were combined into events. To exclude the remaining spikes and some events generated by background spikes, a t_{off} threshold was set. For spikes with negative ΔI, the merged events with a t_{off} < 10 ms were ignored. For spikes with positive ΔI, the merged events with a t_{off} < 4 ms were ignored. Additional validation involved signal-to-noise ratio criteria. Events whose $SD > 3 \times SD\ (I_0)$ ($SD\ (I_0)$ is the standard deviation of the open pore current) or $\Delta I > 3 \times SD\ (I_0)$ were reserved as valid events.

Characteristic parameters of valid events including $\Delta I/I_0$, SD, t_{off}, t_{on}, $\Delta I_{20}/I_0$ and SD_{20} were further calculated. DBSCAN (density-based spatial clustering of applications with noise) analysis was employed to remove nonclustered events. Events from background were manually removed. Data visualization and statistical analyses including histogram plots, scatter plots and curve fittings were conducted using Origin 2021. Machine learning was performed by the Classification Learner toolbox of MATLAB R2021a. A total of 500 valid events from each biogenic amine (BA) class were collected to form a data set, with each event characterized by four features ($\Delta I/I_0$, SD, $\Delta I_{20}/I_0$ and SD_{20}). Each event was labeled according to the corresponding BA type used for data generation. The labeled data set was then randomly split into a training set (80%, 400 samples per label) and a testing set (20%, 100 samples per label) for model training and testing, respectively. A series of inbuilt classifiers of MATLAB, including Decision Trees, Discriminant Analysis, Naive Bayes, Support Vector Machine (SVM), K-Nearest Neighbor (KNN), Ensemble and Neural Network were evaluated. The Bagging Tree model reported the best testing accuracy and was selected for further event prediction.

BA Detection in Shrimp by MspA-NTA-Ni

Shrimp samples were purchased from the local market, then shelled and allowed to naturally rot under ambient conditions for 7 days. Subsequently, 1.8 g of rotten shrimp was processed with 4 mL of 0.4 M trichloroacetic acid (TCA) via mechanical crushing for 10 min to facilitate BA extraction. The resultant extract was adjusted to a pH range of 8−9 using KOH, followed by centrifugation at 13,000 rpm for 10 min. Then, 10 μL of supernatant was added to the *trans* side of MspA-NTA-Ni to initiate nanopore measurement. The concentrated sample is prepared by adjusting pH to ∼12 and extracting by *n*-butanol/trichloromethane (1:1). Then, adjust the pH of the organic phase to ∼5, dry it with nitrogen, and dissolve it in 50 μL water. Five μL sample was added to the *trans* side of MspA-NTA-Ni to initiate nanopore measurement. A 1.5 M KCl buffer (1.5 M KCl, 200 mM CHES, pH 9.0) was used and a transmembrane potential of +100 mV was continuously applied. The BA events were extracted and subsequently identified by the pretrained Bagging Tree model.

■ ASSOCIATED CONTENT

Supporting Information

The Supporting Information is available free of charge at https://pubs.acs.org/doi/10.1021/acsnano.5c16056.

Simultaneous sensing of biogenic amine mixture (MP4)

Materials, statistics of event core parameters, continuous current traces during single-channel recordings, histograms of various parameters and scatter plots (PDF)

■ AUTHOR INFORMATION

Corresponding Authors

Shuo Huang − *State Key Laboratory of Analytical Chemistry for Life Sciences, School of Chemistry and Chemical Engineering, Nanjing University, 210023 Nanjing, China; Chemistry and Biomedicine Innovation Center (ChemBIC), Nanjing University, 210023 Nanjing, China;* orcid.org/0000-0001-6133-7027; Email: shuo.huang@nju.edu.cn

Kefan Wang − *State Key Laboratory of Analytical Chemistry for Life Sciences, School of Chemistry and Chemical Engineering, Nanjing University, 210023 Nanjing, China; Chemistry and Biomedicine Innovation Center (ChemBIC), Nanjing*

https://doi.org/10.1021/acsnano.5c16056
ACS Nano 2026, 20, 2740−2751

University, 210023 Nanjing, China; orcid.org/0000-0001-8932-2660; Email: kfwang@nju.edu.cn

Authors

Yunqi Xiao − *State Key Laboratory of Analytical Chemistry for Life Sciences, School of Chemistry and Chemical Engineering, Nanjing University, 210023 Nanjing, China; Chemistry and Biomedicine Innovation Center (ChemBIC), Nanjing University, 210023 Nanjing, China;* orcid.org/0000-0003-1473-9036

Xiaoyu Du − *State Key Laboratory of Analytical Chemistry for Life Sciences, School of Chemistry and Chemical Engineering, Nanjing University, 210023 Nanjing, China; Chemistry and Biomedicine Innovation Center (ChemBIC), Nanjing University, 210023 Nanjing, China;* orcid.org/0000-0002-4553-8205

Lulu Zhao − *State Key Laboratory of Analytical Chemistry for Life Sciences, School of Chemistry and Chemical Engineering, Nanjing University, 210023 Nanjing, China; Chemistry and Biomedicine Innovation Center (ChemBIC), Nanjing University, 210023 Nanjing, China*

Xinyi Dai − *State Key Laboratory of Analytical Chemistry for Life Sciences, School of Chemistry and Chemical Engineering, Nanjing University, 210023 Nanjing, China; Chemistry and Biomedicine Innovation Center (ChemBIC), Nanjing University, 210023 Nanjing, China*

Lu Qian − *State Key Laboratory of Analytical Chemistry for Life Sciences, School of Chemistry and Chemical Engineering, Nanjing University, 210023 Nanjing, China; Chemistry and Biomedicine Innovation Center (ChemBIC), Nanjing University, 210023 Nanjing, China*

Shanyu Zhang − *State Key Laboratory of Analytical Chemistry for Life Sciences, School of Chemistry and Chemical Engineering, Nanjing University, 210023 Nanjing, China; Chemistry and Biomedicine Innovation Center (ChemBIC), Nanjing University, 210023 Nanjing, China*

Panke Zhang − *State Key Laboratory of Analytical Chemistry for Life Sciences, School of Chemistry and Chemical Engineering, Nanjing University, 210023 Nanjing, China;* orcid.org/0000-0001-8562-9972

Complete contact information is available at: https://pubs.acs.org/10.1021/acsnano.5c16056

Author Contributions

[§]Y.X. and X.D. contributed equally to this work. S.H., Y.X., K.F.W. and X.D. conceived the project. Y.X., X.D., L.Z., X.D. and L.Q. performed the measurements. S.Z. and K.F.W. performed the pore engineering. Y.X. designed the machine learning algorithms. P.Z. set up the instruments. S.H., Y.X., and K.F.W. wrote the paper. S.H. supervised the project.

Funding

This project was funded by the National Key R&D Program of China (Grant No. 2022YFA1304602), National Natural Science Foundation of China (Grant No. 22225405, 22534004), the Fundamental Research Funds for the Central Universities (Grant No. 020514380336), State Key Laboratory of Analytical Chemistry for Life Science (Grant No. 5431ZZXM2509), National Natural Science Foundation of China (Grant No. 223B2402, to K.F.W.). China National Postdoctoral Program for Innovative Talents (Grant No. BX20250087, to K.F.W.). Jiangsu Funding Program for Excellent Postdoctoral Talent (Grant No. 2025ZB212, to K.F.W.).

Notes

This study was formally exempted from ethical review by the Science and Technology Ethics Committee of Nanjing University. All shrimp samples (*Penaeus orientalis*) used in this study were purchased from a commercial supermarket as food-grade materials, and no live animals were involved.

The authors declare the following competing financial interest(s): S.H., S.Y.Z. and K.F.W. have filed patents describing the preparation of heterogeneous MspA and its applications thereof. The remaining authors declare no competing interests.

■ ABBREVIATIONS

BAs, biogenic amines; TLC, thin-layer chromatography; HPLC, high-performance liquid chromatography; MALDI-MS, matrix-assisted laser desorption/ionization mass spectrometry; CE, capillary electrophoresis; α-HL, α-hemolysin; MspA, *Mycobacterium smegmatis* porin A; PUT, putrescine; CAD, cadaverine; HIS, histamine; PHE, β-phenylethylamine; TYR, tyramine; TRP, tryptamine.

■ REFERENCES

(1) Santos, M. H. S. Biogenic Amines: Their Importance in Foods. *Int. J. Food Microbiol.* **1996**, *29*, 213−231.

(2) Linares, D. M.; Martín, M.; Ladero, V.; Alvarez, M. A.; Fernández, M. Biogenic Amines in Dairy Products. *Crit. Rev. Food Sci. Nutr.* **2011**, *51*, 691−703.

(3) Ruiz-Capillas, C.; Jiménez-Colmenero, F. Biogenic Amines in Meat and Meat Products. *Crit. Rev. Food Sci. Nutr.* **2004**, *44*, 489−599.

(4) Prester, L. Biogenic Amines in Fish, Fish Products and Shellfish: A Review. *Food Addit. Contam.,: Part A* **2011**, *28*, 1547−1560.

(5) Doeun, D.; Davaatseren, M.; Chung, M.-S. Biogenic Amines in Foods. *Food Sci. Biotechnol.* **2017**, *26*, 1463−1474.

(6) Ahmad, W.; Mohammed, G. I.; Al-Eryani, D. A.; Saigl, Z. M.; Alyoubi, A. O.; Alwael, H.; Bashammakh, A. S.; O'Sullivan, C. K.; El-Shahawi, M. S. Biogenic Amines Formation Mechanism and Determination Strategies: Future Challenges and Limitations. *Crit. Rev. Anal. Chem.* **2020**, *50*, 485−500.

(7) Romano, A.; Klebanowski, H.; La Guerche, S.; Beneduce, L.; Spano, G.; Murat, M.-L.; Lucas, P. Determination of Biogenic Amines in Wine by Thin-Layer Chromatography/Densitometry. *Food Chem.* **2012**, *135*, 1392−1396.

(8) Bockhardt, A.; Krause, I.; Klostermeyer, H. Determination of Biogenic Amines by RP-HPLC of the Dabsyl Derivates. *Z. Lebensm.-Unters. Forsch.* **1996**, *203*, 65−70.

(9) Gatti, R.; Lotti, C.; Morigi, R.; Andreani, A. Determination of Octopamine and Tyramine Traces in Dietary Supplements and Phytoextracts by High Performance Liquid Chromatography after Derivatization with 2,5-Dimethyl-1H-Pyrrole-3,4-Dicarbaldehyde. *J. Chromatogr. A* **2012**, *1220*, 92−100.

(10) Peña-Gallego, A.; Hernández-Orte, P.; Cacho, J.; Ferreira, V. High-Performance Liquid Chromatography Analysis of Amines in Must and Wine: A Review. *Food Rev. Int.* **2012**, *28*, 71−96.

(11) Su, H.-H.; Chuang, L.-Y.; Tseng, W.-L.; Lu, C.-Y. Micro-Scale Strategy to Detect Spermine and Spermidine by MALDI−TOF MS in Foods and Identification of Apoptosis-Related Proteins by Nano-Flow UPLC−MS/MS after Treatment with Spermine and Spermidine. *J. Chromatogr. B* **2015**, *978*−*979*, 131−137.

(12) Marks Rupp, H. S.; Anderson, C. R. Rapid Determination and Confirmation of Biogenic Amines in Tuna Loin by Gas Chromatography/Mass Spectrometry Using Ethylchloroformate Derivative. *J. AOAC Int.* **2006**, *89*, 1591−1599.

(13) Parchami, R.; Kamalabadi, M.; Alizadeh, N. Determination of Biogenic Amines in Canned Fish Samples Using Head-Space Solid Phase Microextraction Based on Nanostructured Polypyrrole Fiber Coupled to Modified Ionization Region Ion Mobility Spectrometry. *J. Chromatogr. A* **2017**, *1481*, 37−43.

(14) Hlabangana, L.; Hernández-Cassou, S.; Saurina, J. Determination of Biogenic Amines in Wines by Ion-Pair Liquid Chromatography and Post-Column Derivatization with 1,2-Naphthoquinone-4-Sulphonate. *J. Chromatogr. A* **2006**, *1130*, 130−136.
(15) Romero, R.; Gázquez, D.; Bagur, M. G.; Sánchez-Viñas, M. Optimization of Chromatographic Parameters for the Determination of Biogenic Amines in Wines by Reversed-Phase High-Performance Liquid Chromatography. *J. Chromatogr. A* **2000**, *871*, 75−83.
(16) Calull, M.; Marcé, R. M.; Fábregas, J.; Borrull, F. A Method for the Determination of Histamine in Wine by HPLC with Precolumn Derivatization with Phenylisothiocyanate. *Chromatographia* **1991**, *31*, 133−136.
(17) Hernández-Orte, P.; Peña-Gallego, A.; Ibarz, M. J.; Cacho, J.; Ferreira, V. Determination of the Biogenic Amines in Musts and Wines before and after Malolactic Fermentation Using 6-Aminoquinolyl-N-Hydroxysuccinimidyl Carbamate As the Derivatizing Agent. *J. Chromatogr. A* **2006**, *1129*, 160−164.
(18) Lozanov, V.; Petrov, S.; Mitev, V. Simultaneous Analysis of Amino Acid and Biogenic Polyamines by High-Performance Liquid Chromatography after Pre-Column Derivatization with N-(9-Fluorenylmethoxycarbonyloxy)Succinimide. *J. Chromatogr. A* **2004**, *1025*, 201−208.
(19) Kirschbaum, J.; Busch, I.; Brückner, H. Determination of Biogenic Amines in Food by Automated Pre-Column Derivatization with 2-Naphthyloxycarbonyl Chloride (NOC-Cl). *Chromatographia* **1997**, *45*, 263−268.
(20) Adamou, R.; Coly, A.; Douabalé, S. E.; Saleck, M. L. O. C. O.; Gaye-Seye, M. D.; Tine, A. Fluorimetric Determination of Histamine in Fish Using Micellar Media and Fluorescamine As Labelling Reagent. *J. Fluoresc.* **2005**, *15*, 679−688.
(21) Ma, S.; Wang, Y.; Jiang, L.; Hu, R.; Luo, Z.; Li, G. Solid-Contact Ion-Selective Electrodes for Potentiometric Determination of Phenylethylamine in Vitro. *Meas. Sci. Technol.* **2021**, *32*, No. 115116.
(22) Ho, L. S. J.; Fogel, R.; Limson, J. L. Generation and Screening of Histamine-Specific Aptamers for Application in a Novel Impedimetric Aptamer-Based Sensor. *Talanta* **2020**, *208*, No. 120474.
(23) Xia, H.-q.; Kitazumi, Y.; Shirai, O.; Ohta, H.; Kurihara, S.; Kano, K. Putrescine Oxidase/Peroxidase-Co-Immobilized and Mediator-Less Mesoporous Microelectrode for Diffusion-Controlled Steady-State Amperometric Detection of Putrescine. *J. Electroanal. Chem.* **2017**, *804*, 128−132.
(24) Adımcılar, V.; Öztekin, N.; Erim, F. B. A Direct and Sensitive Analysis Method for Biogenic Amines in Dairy Products by Capillary Electrophoresis Coupled with Contactless Conductivity Detection. *Food Anal. Methods* **2018**, *11*, 1374−1379.
(25) Kovács, Á.; Simon-Sarkadi, L.; Ganzler, K. Determination of Biogenic Amines by Capillary Electrophoresis. *J. Chromatogr. A* **1999**, *836*, 305−313.
(26) Sun, X.; Yang, X.; Wang, E. Determination of Biogenic Amines by Capillary Electrophoresis with Pulsed Amperometric Detection. *J. Chromatogr. A* **2003**, *1005*, 189−195.
(27) Kvasnička, F.; Voldřich, M. Determination of Biogenic Amines by Capillary Zone Electrophoresis with Conductometric Detection. *J. Chromatogr. A* **2006**, *1103*, 145−149.
(28) Kashyap, S.; Tehri, N.; Verma, N.; Gahlaut, A.; Hooda, V. Recent Advances in Development of Electrochemical Biosensors for the Detection of Biogenic Amines. *3 Biotech* **2023**, *13*, No. 2.
(29) Zhao, X.; Zhang, Y.; Qing, G. Nanopore toward Genuine Single-Molecule Sensing: Molecular Ping-Pong Technology. *Nano Lett.* **2025**, *25*, 3692−3706.
(30) Wang, Y.; Zhang, S.; Jia, W.; Fan, P.; Wang, L.; Li, X.; Chen, J.; Cao, Z.; Du, X.; Liu, Y.; Wang, K.; Hu, C.; Zhang, J.; Hu, J.; Zhang, P.; Chen, H.-Y.; Huang, S. Identification of Nucleoside Monophosphates and Their Epigenetic Modifications Using an Engineered Nanopore. *Nat. Nanotechnol.* **2022**, *17*, 976−983.
(31) Wang, Y.; Fan, P.; Zhang, S.; Wang, L.; Li, X.; Jia, W.; Liu, Y.; Wang, K.; Du, X.; Zhang, P.; Huang, S. Discrimination of Ribonucleoside Mono-, Di-, and Triphosphates Using an Engineered Nanopore. *ACS Nano* **2022**, *16*, 21356−21365.
(32) Boersma, A. J.; Bayley, H. Continuous Stochastic Detection of Amino Acid Enantiomers with a Protein Nanopore. *Angew. Chem., Int. Ed.* **2012**, *51*, 9606−9609.
(33) Yuan, B.; Li, S.; Ying, Y.-L.; Long, Y.-T. The analysis of single cysteine molecules with an aerolysin nanopore. *Analyst* **2020**, *145*, 1179−1183.
(34) Wei, X.; Ma, D.; Zhang, Z.; Wang, L. Y.; Gray, J. L.; Zhang, L.; Zhu, T.; Wang, X.; Lenhart, B. J.; Yin, Y.; Wang, Q.; Liu, C. N-Terminal Derivatization-Assisted Identification of Individual Amino Acids Using a Biological Nanopore Sensor. *ACS Sens.* **2020**, *5*, 1707−1716.
(35) Wang, Y.; Guan, X.; Zhang, S.; Liu, Y.; Wang, S.; Fan, P.; Du, X.; Yan, S.; Zhang, P.; Chen, H.-Y.; Li, W.; Zhang, D.; Huang, S. Structural-Profiling of Low Molecular Weight RNAs by Nanopore Trapping/Translocation Using Mycobacterium Smegmatis Porin A. *Nat. Commun.* **2021**, *12*, No. 3368.
(36) Clarke, J.; Wu, H.-C.; Jayasinghe, L.; Patel, A.; Reid, S.; Bayley, H. Continuous Base Identification for Single-Molecule Nanopore DNA Sequencing. *Nat. Nanotechnol.* **2009**, *4*, 265−270.
(37) Cao, C.; Cirauqui, N.; Marcaida, M. J.; Buglakova, E.; Duperrex, A.; Radenovic, A.; Dal Peraro, M. Single-Molecule Sensing of Peptides and Nucleic Acids by Engineered Aerolysin Nanopores. *Nat. Commun.* **2019**, *10*, No. 4918.
(38) Ahmad, M.; Ha, J.-H.; Mayse, L. A.; Presti, M. F.; Wolfe, A. J.; Moody, K. J.; Loh, S. N.; Movileanu, L. A Generalizable Nanopore Sensor for Highly Specific Protein Detection at Single-Molecule Precision. *Nat. Commun.* **2023**, *14* (1), No. 1374.
(39) Li, M.; Xiong, Y.; Cao, Y.; Zhang, C.; Li, Y.; Ning, H.; Liu, F.; Zhou, H.; Li, X.; Ye, X.; Pang, Y.; Zhang, J.; Liang, X.; Qing, G. Identification of Tagged Glycans with a Protein Nanopore. *Nat. Commun.* **2023**, *14*, No. 1737.
(40) Xia, K.; Hagan, J. T.; Fu, L.; Sheetz, B. S.; Bhattacharya, S.; Zhang, F.; Dwyer, J. R.; Linhardt, R. J. Synthetic Heparan Sulfate Standards and Machine Learning Facilitate the Development of Solid-State Nanopore Analysis. *Proc. Natl. Acad. Sci. U.S.A.* **2021**, *118*, No. e2022806118.
(41) Ali, M.; Ramirez, P.; Duznovic, I.; Nasir, S.; Mafe, S.; Ensinger, W. Label-Free Histamine Detection with Nanofluidic Diodes through Metal Ion Displacement Mechanism. *Colloids Surf., B* **2017**, *150*, 201−208.
(42) Nakatsuka, N.; Faillétaz, A.; Eggemann, D.; Forró, C.; Vörös, J.; Momotenko, D. Aptamer Conformational Change Enables Serotonin Biosensing with Nanopipettes. *Anal. Chem.* **2021**, *93*, 4033−4041.
(43) Zhao, T.; Wang, J.-W.; Zhang, H.-S.; Zheng, X.; Chen, Y.-P.; Tang, H.; Jiang, J.-H. Development of Dual-Nanopore Biosensors for Detection of Intracellular Dopamine and Dopamine Efflux from Single PC12 Cell. *Anal. Chem.* **2022**, *94*, 15541−15545.
(44) Ding, Y.; Fleming, A. M.; Burrows, C. J. α-Hemolysin Nanopore Studies Reveal Strong Interactions between Biogenic Polyamines and DNA Hairpins. *Microchim. Acta* **2016**, *183*, 973−979.
(45) Boersma, A. J.; Brain, K. L.; Bayley, H. Real-Time Stochastic Detection of Multiple Neurotransmitters with a Protein Nanopore. *ACS Nano* **2012**, *6*, 5304−5308.
(46) Niederweis, M.; Ehrt, S.; Heinz, C.; Klöcker, U.; Karosi, S.; Swiderek, K. M.; Riley, L. W.; Benz, R. Cloning of the MspA Gene Encoding a Porin from Mycobacterium Smegmatis. *Mol. Microbiol.* **1999**, *33*, 933−945.
(47) Faller, M.; Niederweis, M.; Schulz, G. E. The Structure of a Mycobacterial Outer-Membrane Channel. *Science* **2004**, *303*, 1189−1192.
(48) Butler, T. Z.; Pavlenok, M.; Derrington, I. M.; Niederweis, M.; Gundlach, J. H. Single-Molecule DNA Detection with an Engineered MspA Protein Nanopore. *Proc. Natl. Acad. Sci. U.S.A.* **2008**, *105*, 20647−20652.
(49) Cao, J.; Jia, W.; Zhang, J.; Xu, X.; Yan, S.; Wang, Y.; Zhang, P.; Chen, H.-Y.; Huang, S. Giant Single Molecule Chemistry Events Observed from a Tetrachloroaurate(III) Embedded Mycobacterium Smegmatis Porin A Nanopore. *Nat. Commun.* **2019**, *10*, No. 5668.
(50) Wang, S.; Cao, J.; Jia, W.; Guo, W.; Yan, S.; Wang, Y.; Zhang, P.; Chen, H.-Y.; Huang, S. Single Molecule Observation of Hard-Soft-

https://doi.org/10.1021/acsnano.5c16056
ACS Nano 2026, 20, 2740−2751

Acid-Base (HSAB) Interaction in Engineered Mycobacterium Smegmatis Porin A (MspA) Nanopores. *Chem. Sci.* **2020**, *11*, 879−887.
(51) Zhang, S.; Cao, Z.; Fan, P.; Wang, Y.; Jia, W.; Wang, L.; Wang, K.; Liu, Y.; Du, X.; Hu, C.; Zhang, P.; Chen, H.-Y.; Huang, S. A Nanopore-Based Saccharide Sensor. *Angew. Chem., Int. Ed.* **2022**, *61*, No. e202203769.
(52) Liu, Y.; Zhang, S.; Wang, Y.; Wang, L.; Cao, Z.; Sun, W.; Fan, P.; Zhang, P.; Chen, H.-Y.; Huang, S. Nanopore Identification of Alditol Epimers and Their Application in Rapid Analysis of Alditol-Containing Drinks and Healthcare Products. *J. Am. Chem. Soc.* **2022**, *144*, 13717−13728.
(53) Wang, K.; Zhang, S.; Zhou, X.; Yang, X.; Li, X.; Wang, Y.; Fan, P.; Xiao, Y.; Sun, W.; Zhang, P.; Li, W.; Huang, S. Unambiguous Discrimination of All 20 Proteinogenic Amino Acids and Their Modifications by Nanopore. *Nat. Methods* **2024**, *21*, 92−101.
(54) Ouyang, Y.; Wang, K.; Jia, W.; Zhang, P.; Huang, S. Simultaneous Identification of Vitamins B1, B3, B5, and B6 by an Engineered Nanopore. *Nano Lett.* **2024**, *24*, 11944−11953.
(55) Wang, K.; Yang, X.; Xiao, Y.; Cao, Z.; Zhang, S.; Zhang, P.; Huang, S. Simultaneous Identification of Major Thyroid Hormones by a Nickel Immobilized Biological Nanopore. *Nano Lett.* **2024**, *24*, 305−311.
(56) Bulushi, I. A.; Poole, S.; Deeth, H. C.; Dykes, G. A. Biogenic Amines in Fish: Roles in Intoxication, Spoilage, and Nitrosamine Formation—A Review. *Crit. Rev. Food Sci. Nutr.* **2009**, *49*, 369−377.
(57) Shalaby, A. R. Significance of Biogenic Amines to Food Safety and Human Health. *Food Res. Int.* **1996**, *29*, 675−690.
(58) Maintz, L.; Novak, N. Histamine and Histamine Intolerance. *Am. J. Clin. Nutr.* **2007**, *85*, 1185−1196.
(59) Lee, Y.-J.; Kim, H. R.; Lee, C. Y.; Hyun, S.-A.; Ko, M. Y.; Lee, B.-S.; Hwang, D. Y.; Ka, M. 2-Phenylethylamine (PEA) Ameliorates Corticosterone-Induced Depression-Like Phenotype via the BDNF/TrkB/CREB Signaling Pathway. *Int. J. Mol. Sci.* **2020**, *21*, No. 9103.
(60) McCabe-Sellers, B. J.; Staggs, C. G.; Bogle, M. L. Tyramine in Foods and Monoamine Oxidase Inhibitor Drugs: A Crossroad Where Medicine, Nutrition, Pharmacy, and Food Industry Converge. *J. Food Compos. Anal.* **2006**, *19*, S58−S65.
(61) Jones, R. S. G. Tryptamine: A Neuromodulator or Neurotransmitter in Mammalian Brain? *Prog. Neurobiol.* **1982**, *19*, 117−139.
(62) Önal, A. A Review: Current Analytical Methods for the Determination of Biogenic Amines in Foods. *Food Chem.* **2007**, *103*, 1475−1486.
(63) Huang, G.; Willems, K.; Soskine, M.; Wloka, C.; Maglia, G. Electro-Osmotic Capture and Ionic Discrimination of Peptide and Protein Biomarkers with FraC Nanopores. *Nat. Commun.* **2017**, *8*, No. 935.
(64) Chinappi, M.; Yamaji, M.; Kawano, R.; Cecconi, F. Analytical Model for Particle Capture in Nanopores Elucidates Competition among Electrophoresis, Electroosmosis, and Dielectrophoresis. *ACS Nano* **2020**, *14*, 15816−15828.
(65) Bajaj, H.; Gutierrez, S. A.; Bodrenko, I.; Malloci, G.; Scorciapino, M. A.; Winterhalter, M.; Ceccarelli, M. Bacterial Outer Membrane Porins As Electrostatic Nanosieves: Exploring Transport Rules of Small Polar Molecules. *ACS Nano* **2017**, *11*, 5465−5473.
(66) Baldelli, M.; Di Muccio, G.; Sauciuc, A.; della Rocca, B. M.; Viola, F.; Balme, S.; Bonini, A.; Maglia, G.; Chinappi, M. Controlling Electroosmosis in Nanopores Without Altering the Nanopore Sensing Region. *Adv. Mater.* **2024**, *36*, No. 2401761.
(67) Boukhet, M.; Piguet, F.; Ouldali, H.; Pastoriza-Gallego, M.; Pelta, J.; Oukhaled, A. Probing Driving Forces in Aerolysin and α-Hemolysin Biological Nanopores: Rlectrophoresis Versus Electroosmosis. *Nanoscale* **2016**, *8*, 18352−18359.

https://doi.org/10.1021/acsnano.5c16056
ACS Nano 2026, 20, 2740−2751